Hindawi
Applied Bionics and Biomechanics
Volume 2022, Article ID 6110482, 12 pages
https://doi.org/10.1155/2022/6110482

Research Article

Modeling and Analysis of Prostate Soft Tissue Puncture Performance using Puncture Needle

Bing Li[1] **and Lipeng Yuan**[2]

[1]*School of Mechanical Power Engineering, Harbin University of Science and Technology, Harbin 150080, China*
[2]*School of Mechanical Engineering, Harbin Institute of Technology, Harbin 150010, China*

Correspondence should be addressed to Lipeng Yuan; hitylp@126.com

Received 17 February 2022; Revised 6 September 2022; Accepted 12 October 2022; Published 2 December 2022

Academic Editor: Qiguo Rong

When treating prostate cancer, the use of puncture robots is an effective method to perform radioactive seed implantation surgery. However, when the puncture needle enters the lesion, the soft tissue is easily deformed owing to the complex force between the puncture needle and soft tissue, which leads to a puncture deviation between the needle tip and target point. To solve this problem effectively, the prostate soft tissue puncture process is studied based on the analysis of the puncture needle–soft tissue interaction. First, the puncture force is classified into contact, friction, and cutting forces by a quantitative decomposition method, and the corresponding force model is established. Based on the theoretical analysis of the model, it is deduced that these factors can affect the deformation created by puncturing the soft tissue. Subsequently, a puncture platform is built and many biomimetic soft tissue models are established. Multiple puncture experiments on the influencing factors are conducted using the method of controlling a single variable. Using the spatial puncture deviation as the test metrics, the significance of the influencing factors of the puncture deformation is verified. Finally, it can be concluded from the experimental analysis that the main factor that affects the puncture deviation is the puncture speed, whereas the puncture depth has no significant influence. The puncture speed was optimized and verified by experiments, and the results showed that a stable puncture accuracy under different puncture depths can be obtained by selecting an optimized puncture speed (12.6 mm/s). This work provides a design reference to study the positioning accuracy of minimally invasive puncture surgery.

1. Introduction

Presently, cancer is a significant life-threatening disease. According to survey data from the International Agency for Research on Cancer by the World Health Organization in 2020, the number of new cancer cases in the world would reach 19.29 million in 2021, and the male cases would reach 10.06 million [1–3]. There are 1.41 million new cases of prostate cancer, accounting for 7.3% of the total number of new cancer cases [4–8]. Particularly, prostate cancer has been a threat to human's life. Radioactive seed implantation surgery is an important method for the treatment of prostate cancer. Compared with systemic chemotherapy, immunotherapy, external radiotherapy, and surgical treatment, this method offers the advantages of low soft tissue damage, high surgical safety, and reproducibility [9]. Therefore, radioactive seed implantation surgery has become the main method for the treatment of prostate cancer [10].

In recent years, with the rapid development of the robotics industry, robotic technologies have been increasingly used in clinical operations, and medical robots are gradually being accepted by patients and doctors. Therefore, minimally invasive interventional surgical robot technology is the most promising key technology in the field of medical robots in the future. The Da Vinci robot developed by the American Intuition Corporation (Intuitive Surgical (ISRG. US)) is a representative medical robot, which not only possesses a high positioning accuracy and good motion stability but also can continuously replace the work of doctors. This robot causes minimal trauma to patients and facilitates postoperative recovery [11, 12]. Minimally invasive interventional surgical robot technology is used to treat prostate

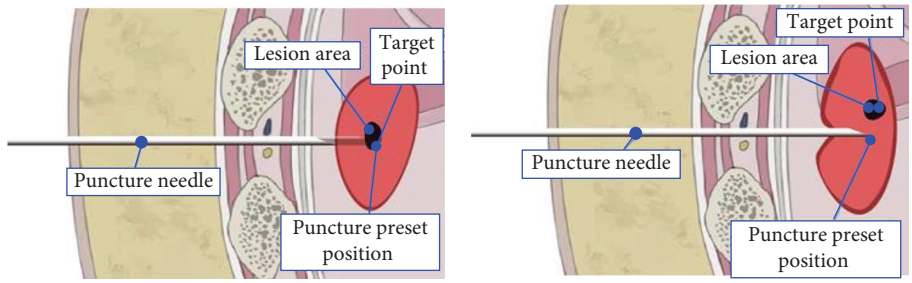

Figure 1: Schematic diagram of tissue deformation during needle–soft tissue interaction: (a) ideal situation of puncture; (b) actual situation of puncture.

cancer by implanting radioactive seeds such as I^{235} and I^{125}. The seed is accurately placed under the specified target point. This reduces the number of punctures and ensures the uniform distribution of dosimetry in the target area. Consequently, postoperative complications are reduced, and the effects of treatment are improved [13]. However, when the robot controls the insertion of the puncture needle into the soft tissue, the interaction between the puncture needle and soft tissue offsets the target in the lesion area, which reduces the accuracy of seed implantation. Therefore, the improvement of the puncture performance of the robot is also a problem that needs to be addressed.

Many scholars have conducted extensive research in this area. Minhas et al. [14] proposed a puncture control method based on a needle body rotation duty cycle. This method could effectively improve the puncture performance by accurately controlling the needle body rotation and needle insertion timed ratio. Majewicz et al. [15] improved the positioning accuracy of the puncture needle by further studying the control method of the needle body alternately rotating around the needle shaft. Sun et al. [16, 17] proposed a fuzzy control method for the puncture speed based on the force/position feedback; when the puncture needle entered a pig liver tissue, the robot automatically stopped the needle until the soft tissue returned to a relaxed state, and then conducted the puncturing at half speed to improve the puncturing accuracy. Liangyi and Zhang et al. [18] designed a high-precision needle insertion strategy based on vibration and rotation to reduce the deviation of the puncture needle in the soft tissue. Webster et al. [19] used needle tips of different angles to penetrate a tissue model and concluded that a smaller needle tip angle led to a greater needle deflection.

The studies by the above scholars were mainly on the reduction of the deflection of the puncture needle by adjusting or changing the different puncture methods. However, in the puncture direction, the displacement error caused by the soft tissue deformation is also the main factor affecting the positioning accuracy, which is rarely reported. Therefore, this study evaluates the main factors affecting the soft tissue deformation and makes reasonable inferences to reduce the positioning error caused by the soft tissue deformation when puncturing prostate soft tissue. The results presented by the above scholars can help to further improve the puncture accuracy. First, this study established a puncture force model between the puncture needle and soft tissue and analyzed the main factors that affected the puncture positioning deviation. Subsequently, multiple puncture experiments on the influencing factors were conducted using the method of controlling a single variable, and the most significant influencing factors were selected. Finally, based on the analysis of the experimental data and theoretical analysis, the parameter values of the significant factors affecting the puncture deviation were optimized, and their feasibility was verified by experiments.

2. Analysis of Soft Tissue Puncture

2.1. Needle–Soft Tissue Interaction. During the puncture stage of the prostate seed implantation surgery, the inner needle should be inserted into the outer needle. The puncture needle is regarded as a solid needle and is inserted into the target lesion area from the pubic region of the human body through the linkage between the inner and outer needles. In the process of implantation, owing to the interaction between the puncture needle and prostate soft tissue, the target point in the lesion area is offset, which requires doctors to adjust the posture of the needle appropriately [20]. This is because the prostate soft tissue is interfered with the external force of the puncture needle during the puncturing process, which causes the deformation of the prostate soft tissue, thereby driving the movement of the lesion area; this causes the target point deviation phenomenon (the amount of deviation between the needle tip and target point in space). Figure 1 shows a schematic diagram of the soft tissue deformation during needle–soft tissue interaction.

2.2. Analysis of the Puncture Process. According to the analysis in Section 2.1, the implantation accuracy of the radioactive seed is affected by the target offset at the puncture stage, and the target offset is mainly affected by the interaction between the needle and prostate soft tissue. Therefore, the entire puncture process should be analyzed.

Biosolids can be divided into hard tissues (such as cartilage and bone) and soft tissues (such as blood vessels, nerves, muscles, and skin). Among them, the hard tissue of the human body has good and relatively fixed mechanical properties, whereas the soft tissue is mostly a viscoelastic body. The prostate is biologically classified as soft tissue, which causes difficulties in the analysis of the prostate puncture

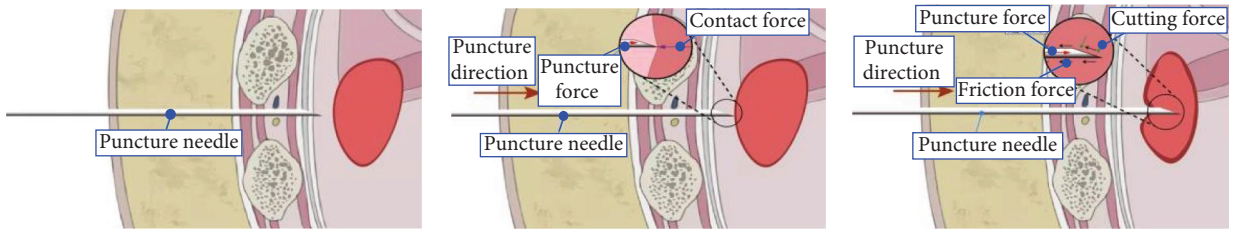

Figure 2: Diagram of puncture process: (a) the puncture needle is not in contact with the prostate soft tissue; (b) the puncture needle begins to contact with the prostate soft tissue; (c) the puncture needle enters the prostate soft tissue.

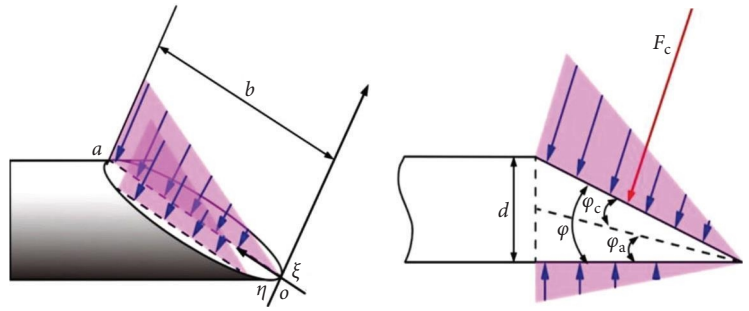

Figure 3: Diagram of force analysis of cutting force: (a) schematic diagram of the needle tip bevel; (b) schematic diagram of the side of the needle tip.

force. For better analysis, the entire puncture process can be divided into three stages [21–23].

(1) The stage where the puncture needle is not in contact with the prostate soft tissue. At this stage, the puncture needle has no contact with the soft tissue or has just reached the contact threshold. Here, the interaction force between the puncture needle and soft tissue is zero. Therefore, there is no change in the prostate soft tissue at this stage as shown in Figure 2(a).

(2) The stage where the puncture needle is in contact with the prostate soft tissue. At this time, the puncture needle is in contact with the soft tissue of the prostate and puts pressure on it, causing the deformation of the prostate. As the puncture needle goes deeper, the fracture stress that the prostate soft tissue can withstand is reached and the surface tissue of the prostate is torn. The puncture needle then penetrates the prostate soft tissue. At this time, the puncture force is equal to the contact force as shown in Figure 2(b). The forces of the needle–soft tissue interaction include the cutting and contact forces.

(3) The stage where the puncture needle enters the prostate soft tissue. In this stage, the needle entering the prostate soft tissue forms a complex force relationship with the soft tissue. The energy overcome by the needle body when implanted into the soft tissue is equal to the potential energy generated by the soft tissue deformation and the irreversible energy generated by the rupture of the damaged soft tissue cells. As shown in Figure 2(c), in this process, the sum of the cutting, friction, and contact forces is equal to the puncture force.

3. Modeling of Prostate Soft Tissue Puncture Force

Through the quantitative analysis of the prostate soft tissue puncture process in the previous section, a puncture force model can be established:

$$f_{\text{puncture}}(\varepsilon) = f_{\text{contact}}(\varepsilon) + f_{\text{cut}}(\varepsilon) + f_{\text{friction}}(\varepsilon), \tag{1}$$

where ε is the depth of the puncture, f_{puncture} is the puncture force, f_{contact} is the contact force, f_{cut} is the cutting force, and f_{friction} is the friction force.

3.1. Modeling of Cutting Force. When the puncture needle enters the prostate soft tissue, the needle tip cuts the original part of the prostate soft tissue and allows the needle body to occupy its cut position. The acting force of the soft tissue is distributed over the bevel of the needle tip of the puncture needle, such that the acting force is the cutting force (f_{cut}), and the inclined plane is the acting surface distributed over an ellipse; its distribution is shown in Figure 3.

The cutting force load ($\delta_{\text{cut}}(\xi)$) is triangularly distributed over the inclined plane, and the distributed load can be expressed as

$$\delta_{\text{cut}}(\xi) = K\xi \tan \varphi_c. \tag{2}$$

The distributed load boundary conditions are expressed as

$$\begin{aligned} \delta_{\text{cut}}(0) &= 0 \\ \delta_{\text{cut}}(b) &= Kb \tan \varphi_c, \end{aligned} \tag{3}$$

where ξ is the contact length between the long axis of the elliptical bevel of the needle tip and the soft tissue when the puncture needle penetrates into the soft tissue, b is the distance from a to o, K is the stiffness of the needle–soft tissue interaction, and φ_c is the cutting angle.

To facilitate the calculation, the o–$\xi\eta$ coordinate system is established on the needle tip bevel. According to the standard ellipse equation, the formula can be expressed as

$$\frac{(\xi - b/2)^2}{(b/2)^2} + \frac{\xi^2}{(d/2)^2} = 1. \tag{4}$$

In the above formula, d is the minor axis on the ellipse of the needle tip (it is also the diameter of the needle). Here, $b = d/\sin\varphi$, and φ is the angle of the needle tip. Therefore, the resultant cutting force received by the entire needle tip is

$$f_{\text{cut}} = \iint_D \delta_{\text{cut}}(\xi) d\xi\, d\eta = 2\int_0^b d\xi \int_0^{\eta(\xi)} \delta_{\text{cut}}(\xi) d\eta, \tag{5}$$

where D is the area of the needle tip bevel of the puncture needle and Equations (2), (3), and (4) are inserted into Equation (5) to solve

$$\begin{aligned} f_{\text{cut}} &= dK \tan \varphi_a \int_0^{d/\sin\varphi} \xi \sqrt{1 - \frac{(\xi - d/2 \sin\varphi)^2}{(d/2 \sin\varphi)^2}} d\xi \\ &= \frac{\pi d^3 K \tan(\varphi - \varphi_c)}{8 \sin^2 \varphi}. \end{aligned} \tag{6}$$

According to Equation (6), the factor affecting the cutting force is the stiffness of the needle–soft tissue interaction. This study assumes that the density of the interactive soft tissue along the puncture needle path is uniform. For puncturing in the same tissue with the same puncture needle, the stiffness of the needle-soft tissue interaction is the same [24]. Therefore, the magnitude of the cutting force is only related to the type of puncture needle installed by the robot. The types of puncture needles, the angle of the needle tip, and the diameter of the puncture needles are different, resulting in different cutting angles, and a change in the puncture force accordingly.

3.2. Modeling of Friction Force. During the puncture process of the seed implantation robot, the friction force between the puncture needle and prostate soft tissue conforms to the Coulomb friction model at low speeds [25]. At high speeds, the generated friction force is closer to the LuGre friction model [24].

(1) At low speed: Because the amount of deformation of the soft tissue is the radius of the needle body, the length-per-unit of the puncture needle body that is subject to the pressure does not change, thus, the equation can be expressed as

$$f_{\text{friction}} = 2\pi d\mu f_n \int_0^{\varepsilon_\lambda} dx, \tag{7}$$

where $\mu = 0.2$ [26], ε_λ is the depth of the puncture needle implantation, and f_n is the pressure of the puncture needle body unit.

According to Equation (7), at low speeds, the frictional force is affected by the implantation depth of the puncture needle and radius of the needle body.

(2) At high speed: Introducing the LuGre friction model, according to ref. [27], it is known that for a larger puncture speed (v_0), the friction force is expressed as

$$\begin{aligned} f_{\text{friction}}(t) &= F_n(u_c + \sigma_2 v_0) \\ u_c &= \sigma_1 v_0 - g(v_0)\text{sgn}(v_0) e^{-\sigma_0 |v_0| t / g(v_0)} + g(v_0)\text{sgn}(v_0), \end{aligned} \tag{8}$$

where u_c is the Coulomb friction coefficient, $g(v_0)$ describes the Stribeck effect, σ_0 is the stiffness coefficient, σ_1 is the damping coefficient, σ_2 is the viscous damping coefficient, and F_n is the radial force of the soft tissue received by the needle.

According to Equation (8), as the puncture speed v_0 increases, the weight of the viscous friction force term $\sigma_2 v_0$ in the friction force gradually increases.

3.3. Modeling of Contact Force. The contact force is the force necessary to tear the boundary of the soft tissue of the prostate, which is generated when the puncture needle contacts the soft tissue of the prostate. The puncture needle enters the prostate soft tissue, and the needle drives the soft tissue of the prostate to move in the direction of the needle. When the fracture stress of the soft tissue is reached, the soft tissue is torn, and the puncture needle enters the prostate soft tissue.

Considering that the prostate soft tissue includes cells and intercellular substances, and the individual cells are different, this reflects the special properties of the prostate soft tissue materials. When the puncture needle is in contact with the prostate soft tissue, it will appear as nonuniform, nonlinear, and plastic. This makes it difficult to analyze the characteristics of the soft tissue at the cellular level when the puncture needle is in contact with the prostate soft tissue. To better describe the biological characteristics of human soft tissues, scholars have used a combination of springs and dampers to build a biomechanical model to analyze the contact force. This method regards the punctured soft tissue as a biological viscoelastic body, and this study uses an improved nonlinear Kelvin model to calculate the contact force during the puncture process. The improved nonlinear Kelvin model has the same structure as the standard Kelvin model; however, the improved one can reflect the nonlinear change characteristics of the soft tissue when the puncture needle is in contact, and can

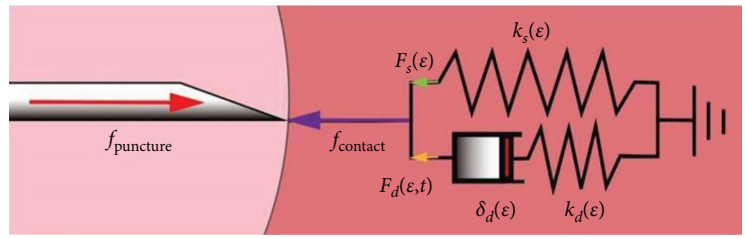

Figure 4: Diagram of contact force analysis.

effectively simulate the biological characteristics of the soft tissue [28–30]. Figure 4 shows the contact force analysis using the improved Kelvin model.

According to Figure 4, the contact force between the puncture needle and soft tissue in the improved Kelvin model is

$$f_{\text{contact}} = F_s(\varepsilon) + F_d(\varepsilon, t), \tag{9}$$

where $F_s(\varepsilon) = k_s(\varepsilon)\varepsilon$ is the contact force component of the spring k_s of the model; $k_s(\varepsilon)$ is the nonlinear spring constant function of the spring k_s; ε is the displacement of the spring; $F_d(\varepsilon,t)$ is the contact force component produced by the model spring $k_d(\varepsilon)$ and the damper $\delta_d(\varepsilon)$.

Because F_d is formed by the series connection of the nonlinear spring k_s and nonlinear damper $\delta_d(\varepsilon)$, according to Newton's third law, the equation can be expressed as

$$F_d = k_d(\varepsilon)\varepsilon_k = \delta_d(\varepsilon)\dot{\varepsilon}_b. \tag{10}$$

The displacement relationship of the series part of the model is then

$$\varepsilon_k + \varepsilon_b = \varepsilon, \tag{11}$$

where ε_k is the displacement of the spring k_d and ε_d is the displacement of the damper δ_d.

It is assumed that k_d and δ_d have the same form in the established model, and the rate of change of the displacement and relaxation time of the model is

$$\tau_c = \frac{k_d(\varepsilon)}{\delta_d(\varepsilon)}. \tag{12}$$

Equations (10) and (11) are combined, and the displacement of the spring can be calculated as

$$\varepsilon_k = \frac{F_d}{k_d(\varepsilon)} = \frac{\delta_d(\varepsilon)}{k_d(\varepsilon)}\dot{\varepsilon}_d(\varepsilon) = \dot{\varepsilon} \cdot \tau_c. \tag{13}$$

The derivative of Equation (11) with respect to time is solved, and combined with (13) to obtain

$$\dot{\varepsilon}_d + \frac{\varepsilon_d}{\tau_c} = \dot{\varepsilon}. \tag{14}$$

According to Equation (14), it can be observed that in the improved Kelvin model, the k_d spring displacement corresponds to a linear differential equation. Its general solution is

$$\varepsilon_k = \int_0^t \dot{\varepsilon}(\tau) e^{\left(-\frac{t-\tau}{\tau}\right)} d\tau. \tag{15}$$

Therefore, the value of F_d is

$$F_d = k(\varepsilon) \int_0^t \dot{\varepsilon}(\tau) e^{\left(-\frac{t-\tau}{\tau_s}\right)} d\tau. \tag{16}$$

Equations (9) and (16) are combined and solved to obtain

$$f_{\text{contact}} = F_s(\varepsilon) + k(\varepsilon)v\tau_s\left(1 - e^{-\varepsilon/v\tau_s}\right). \tag{17}$$

The Taylor series is used to expand (17), and afterward, the contact force expression can be approximated as

$$f_{\text{contact}} = F_s(\varepsilon) + \delta(\varepsilon)\left(\varepsilon - \frac{\varepsilon^2}{2v\tau_s}\right). \tag{18}$$

3.4. Analysis of Puncture Force Model. To sum up, the force model of the puncture action between the puncture needle and soft tissue of the prostate is

$$f_{\text{puncture}} = \begin{cases} f_{\text{contact}}(\varepsilon) = k_s(\varepsilon)\varepsilon + \delta(\varepsilon)\left(\varepsilon - \dfrac{\varepsilon^2}{2v\tau_s}\right) & \varepsilon_1 \le \varepsilon < \varepsilon_2 \\ f_{\text{cut}}(\varepsilon) + f_{\text{friction}}(\varepsilon) = \dfrac{\pi d^3 K \tan(\varphi - \varphi_c)}{8\sin^2\varphi} + \begin{cases} 0.4\pi r\mu f_n\varepsilon & \text{Low speed} \\ F_n(u_c + \sigma_2 v_0) & \text{High speed} \end{cases} & \varepsilon_3 \le \varepsilon < \varepsilon_4, \end{cases} \tag{19}$$

(a) (b)

Figure 5: Models and materials: (a) bionic soft tissue material; (b) bionic soft tissue mode.

where ε_1 is the position when the needle tip touches the soft tissue, ε_2 is the position of the maximum deformation of the soft tissue, ε_3 is the position when the soft tissue begins to break, and ε_4 is the maximum position of the needle when the soft tissue breaks. There is no clear definition between the high-speed and low-speed of the friction part, which shows that different values of the puncture speed can have different effects on friction, which can be verified by subsequent experiments.

It can be observed from Equation (19) that the influencing factors of the needle–soft tissue interaction include the geometric structure of the needle, insertion speed, and implantation depth. The actual situation in seed implantation surgery is considered; doctors should calculate the distribution and dose of radioactive seed in advance according to the condition of the patient. To facilitate puncture planning, doctors use the same seed for implantation as well as the same type of puncture needle. Therefore, only the puncture speed and depth are analyzed on the robot to improve the accuracy of the same and different target points.

During the puncture process, the greater the interaction force between the soft tissue and puncture needle, the greater the deviation between the puncture needle and target point. It can be observed from the above equations that increasing the needle insertion speed can reduce the displacement and deformation of the prostate soft tissue and improve the puncture accuracy. However, an excessively high puncture speed will also affect the friction properties between the puncture needle and soft tissue, which affects the puncture accuracy. Therefore, it is also necessary to analyze the puncture speed to determine an appropriate puncture speed and improve the puncture accuracy. According to Equation (19), the puncture depth also needs to be considered.

4. Research on Needle–Soft Tissue Puncture Experiment

To verify the correctness of the conclusions made in Section 3.4 and determine a suitable effective value of the puncture speed, improve the puncture accuracy, ensure the puncture performance, and meet the best therapeutic effect, this study analyzed a puncture experiment of the needle–soft tissue.

4.1. Experiment Equipment. Presently, the study of prostate soft tissue puncture experiments generally uses silica gel as a bionic soft tissue model [9, 31]. Therefore, this experiment used XB-0920 type silica gel from Xubai New Material Co., Ltd., as shown in Figure 5(a). To better simulate the characteristics of the human prostate soft tissue and calibrate the target point, silica gel (A) and silica gel (B) were mixed. First, these mixed liquids were poured into half the scale of the mold. Second, they were cooled and solidified at normal temperature. Third, the target points were buried in it. Finally, the mixed solution was poured continuously until the bionic soft tissue met the requirements of the experiment. Figure 5(b) shows the silica gel used in the experiment as a bionic soft tissue model.

To approximate the real prostate soft tissue, the bionic soft tissue model used in this experiment was made according to the requirements in ref. [9] (the elastic modulus parameters are consistent).

The puncture platform was used in the experiment as shown in Figure 6. The entire puncture platform includes a measuring camera, an adjustment device, a puncture mechanism, and a vision-processing computer. The puncture platform adjusts the puncture speed when the puncture needle penetrates into the bionic soft tissue through an adjustment device (the maximum value of this speed is 30 mm/s; this value meets the requirements of the experiment). By adjusting the platform to make the bionic soft tissue rise and fall, the tissue is parallel to the needle body, enabling the target point in the bionic soft tissue to align with the axis position of the needle at the beginning of the puncture needle.

In this experiment, the SHLC-200WS industrial camera was used for measurement, and the information obtained by the camera was fed back to the vision-processing computer for processing. The spatial coordinate distance between the tip of the puncture needle and target point was measured and obtained.

4.2. Design of Puncture Experiment. The experiment mainly analyzed the influence of the puncture speed factor on the target offset point. The farthest distance from the perineum to the prostate of Asian adult men is ~50–80 mm. This experiment combined the actual requirements of the prostate puncture operation to design an experimental plan. The

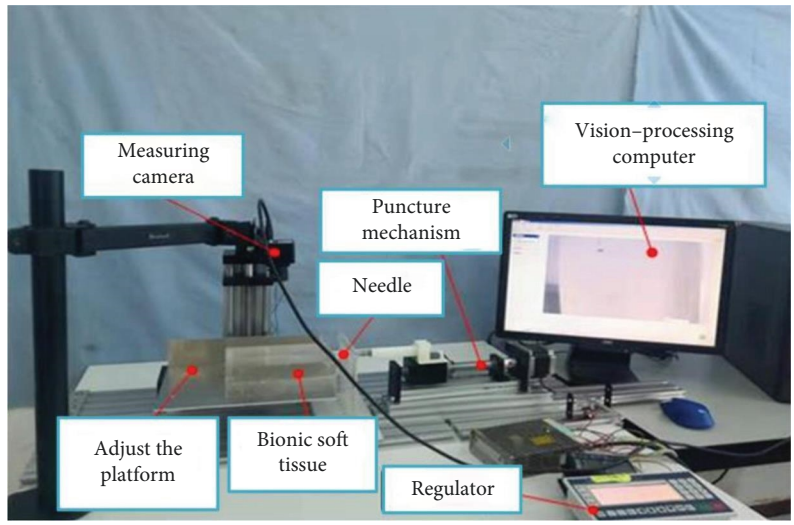

Figure 6: Puncture experiment platform.

Table 1: Range interval of factors.

Factors	Value range of the factors (range interval value of the seven group factors)						
Puncture distance (mm)	50	55	60	65	70	75	80
Puncture speed (mm/s)	2	5	10	15	20	25	30

experiment adopted the analysis of the influence of another factor on the test metrics under the condition that the value of one of the factors remained constant. The test metrics were the puncture deviation values between the puncture needle and target point. The type of puncture needle used was the 18 G standard medical puncture needle.

First, according to the range of the farthest distance from the perineum to the prostate and the speed performance of the puncture platform, the range of parameter values for the two groups of factors were selected as illustrated in Table 1.

The fixed factor method was then selected to conduct an experimental analysis to determine the influence of the two groups of factors on the puncture deviation value, and the optimal value range of the relevant factors.

Finally, to reduce the error of the puncture deviation value measured in the experiment, each group experiment was repeated five times to measure and record the data, and then the five-time average values of the data were obtained.

4.3. Analysis of Experimental Process and Result. Figure 7(a) shows the experimental data for the puncture depths of 50, 55, 60, 65, 70, 75, and 80 mm under puncture speeds of 2, 15, and 30 mm/s. It can be observed from the figure that when the puncture experiments of different depths were performed at the same speed, with the gradual increase of the puncture depths, the puncture deviation between the puncture needle and target point slowly increased; this is because of the cumulative deformation of the bionic soft tissue with the increase of the puncture depth. However, with the gradual increase of the puncture residence time, the variation of the puncture deviation between the puncture needle and target point is not too significant; this is because of the potential energy generated by the deformation of the bionic soft tissue. The puncture friction force between the puncture needle and bionic soft tissue can be overcome under the action of this potential energy, such that the bionic soft tissue itself can gradually recover (rebound phenomenon).

According to the experimental analysis of the different puncture depths at the same puncture speed, it can be deduced that the puncture depth has no significance on the test metrics, whereas the puncture speed has the most significance. Therefore, the experiment of the different puncture speeds was chosen at the same puncture depths in the study (the puncture depth was chosen as 60 mm).

Figure 7(b) shows the test results of the different puncture speed experiments at the same puncture depth. It can be observed from the figure that the deviation value of the target point decreases as the puncture speed increases at the same puncture depth (the puncture speed is 2 –10 mm/s), which is consistent with the previous theoretical analysis. However, when the puncture speed is increased from 10 to 30 mm/s, the puncture deviation (test metrics) begins to increase gradually. Because the bionic soft tissue has viscous and damping characteristics, the weight of the viscous friction force will gradually increase as the speed increases, which further verifies the theoretical analysis.

4.4. Analysis of Parameter Optimization Experiment. According to the experimental analysis in Section 5.3, it can be observed that the main factor that affects the puncture deviation is the puncture speed, and according to Figure 7(b), it can be deduced that the optimal puncture speed range is 10–15 mm/s. However, this discrete interval is relatively large, thus, it needs to be further optimized and analyzed to determine the optimal value of the puncture speed.

Because the speed control accuracy of the puncture platform is 0.1 mm/s, the experiment divided the puncture speed (10–15 mm/s) into 51 groups; the test metrics were still the puncture deviation value, and each group of experiments was

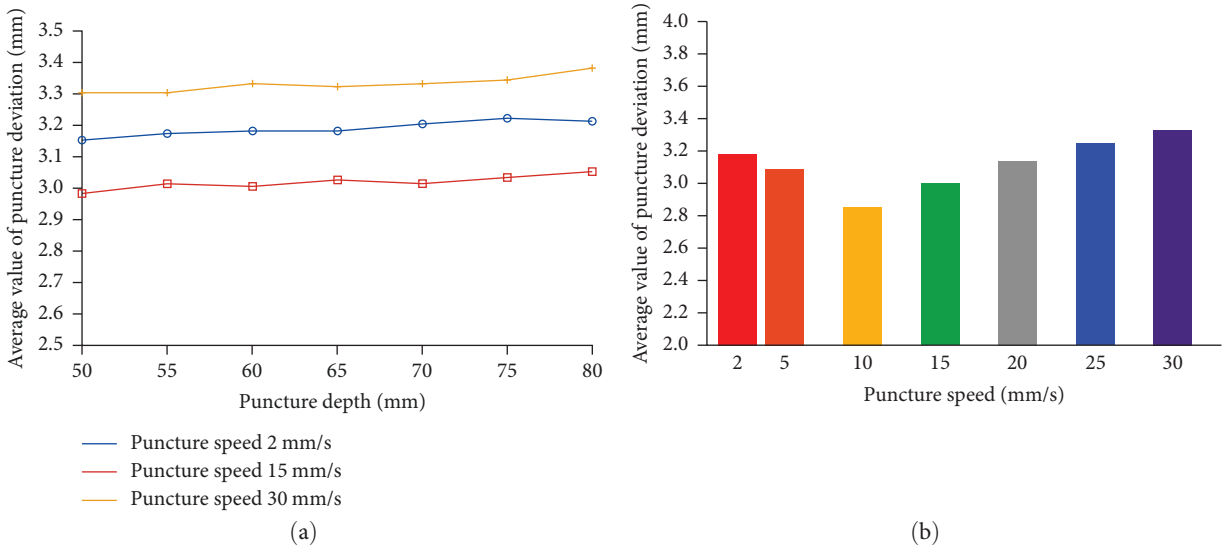

Figure 7: Results of puncture experiment: (a) the effect of the puncture depth; (b) the effect of the puncture speed.

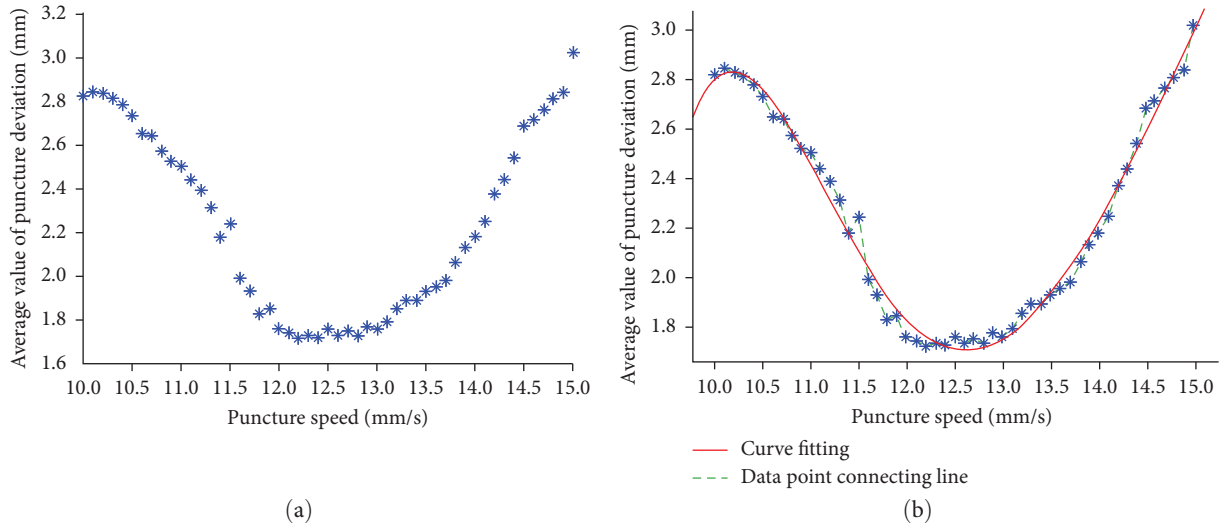

Figure 8: Results of optimization experiments: (a) distribution map of experimental results; (b) curve fitting.

carried out five times. The test results of each group of experiments were averaged. The experimental results are shown in Figure 8(a).

Figure 8(a)shows the discrete points of the experimental data. It can be observed from the previous sections that the puncture speed is within the range of 10–15 mm/s, and the puncture deviation value shows a trend of first a decrease and then an increase. This shows that there is an optimal puncture speed. The minimum value of the puncture deviation is distributed within a puncture speed from 12 to 13 mm/s.

Therefore, to further optimize and determine the best value of the puncture speed, in the first step, the scatter points of the experimental data need to be connected (as shown in Figure 8(b)), and the cubic spline interpolation curve "Polynomial" function of the curve fitting tool "cftool" in MATLAB 2017A software was used to fit the function $f(x)$ relation between the puncture speed and puncture deviation value. It was established as follows:

$$f(x) = p_1x^5 + p_2x^4 + p_3x^3 + p_4x^2 + p_5x^1 + p_6, \tag{20}$$

where $p_1 = 0.003887$, $p_2 = -0.2565$, $p_3 = 7.2$, $p_4 = -96.64$, $p_5 = 640.9$, and $p_6 = -1676$.

The confidence of Equation (20) reaches 98%, R-square: 0.9879 (~1), and as shown in Figure 8(b), the connecting line (red line) of the data is consistent with the discrete data points. Therefore, this study uses the improved adaptive particle swarm algorithm [11, 32] to solve the minimum value of Equation (20), and the optimal puncture speed is obtained as 12.60 mm/s.

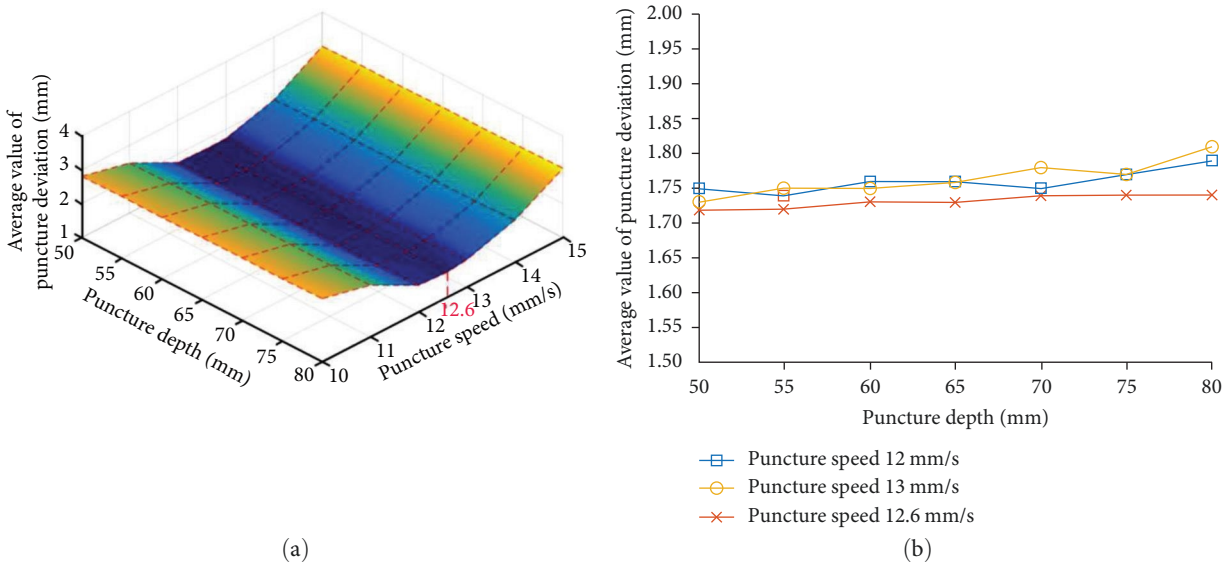

(a) (b)

Figure 9: Results of optimization comparing experiments: (a) overall trend; (b) partial view.

To verify the effectiveness of the obtained optimal puncture speed (12.60 mm/s) in this experiment, it (12.60 mm/s) was compared with 10, 11, 12, 13, 14, and 15 mm/s, as shown in Figure 9.

It can be observed from Figure 9(a) that with the increase of the puncture depth, the puncture deviations with puncture speeds of 12, 12.6, and 13 mm/s are smaller than the other speed conditions. Additionally, Figure 9(b) is a clear expression that the puncture deviation slowly increases as the puncture depth increases, but the puncture deviation with a puncture speed of 12.6 mm/s is smaller than that with a puncture speed of 12 and 13 mm/s.

It can be observed from the experimental results that selecting the puncture speed of 12.6 mm/s for prostate soft tissue puncture can reduce the puncture deviation caused by soft tissue deformation. In the case of different puncturing depths and continuous puncturing, a small puncturing positioning error and relatively stable puncturing accuracy can be maintained.

5. Discussion

When the puncture needle enters the lesion, the soft tissue is easily deformed owing to the complex force between the puncture needle and soft tissue. This deformation leads to a puncture deviation between the needle tip and target point; this problem causes a reduction in the puncture accuracy and affects the treatment effect. Therefore, this study first established a force model between the puncture needle and soft tissue. The main factors that affected the positioning deviation of the puncturing were analyzed, and the appropriate influencing factor parameters were selected to improve the puncture performance. To further illustrate the feasibility and effectiveness of using the force model to analyze related problems, this study listed two groups of similar studies with the same working basis as examples in the discussion part. Du et al. [33] obtained the predicted trajectory of the needle tip in the process of puncturing the soft tissue by establishing the stiffness force model (force model of a spring-supported cantilever beam) of the needle-tissue interaction to experimentally analyze the parameters (the stiffness parameter of the soft tissue to the puncture needle body) affecting the movement trajectory of the puncture needle and improving the puncture performance. Zhang et al. [34] determined the influencing factors affecting the bending deformation of the bevel-tip flexible needle by analyzing the bending force model between the bevel-tip flexible needle and soft tissue, and provided a theoretical basis for improving the puncture positioning accuracy of the bevel-tip flexible needle. Therefore, this study analyzes and studies the problems to be solved by establishing a puncture force model between the puncture needle and soft tissue. It is supported by sufficient theoretical basis and relevant research basis.

When analyzing the procedure of puncturing the prostate soft tissue, the quantitative decomposition method was used to divide the puncture force into contact, friction, and cutting forces, and establish the corresponding force model. By analyzing the force model, a single variable method was used to conduct multiple puncture experiments on the influencing parameters, whereas the spatial puncture deviation was used as the test metrics; it was deduced that the effect of the puncture speed on the puncture deviation was significant. Additionally, the experiment inferred that the puncture depth has no significant influence on the puncture deviation. Therefore, the actual situation of prostate soft tissue puncture surgery is a combination of a reasonable selection of the puncture speed to effectively reduce the soft tissue deformation during the puncture process and improvement of the puncture accuracy and performance. The influence of the puncture depth can be ignored.

The silicone bionic soft tissue used in the experiment was made according to ref. [9] (it is required to approximate the elastic modulus value of human prostate soft tissue as closely

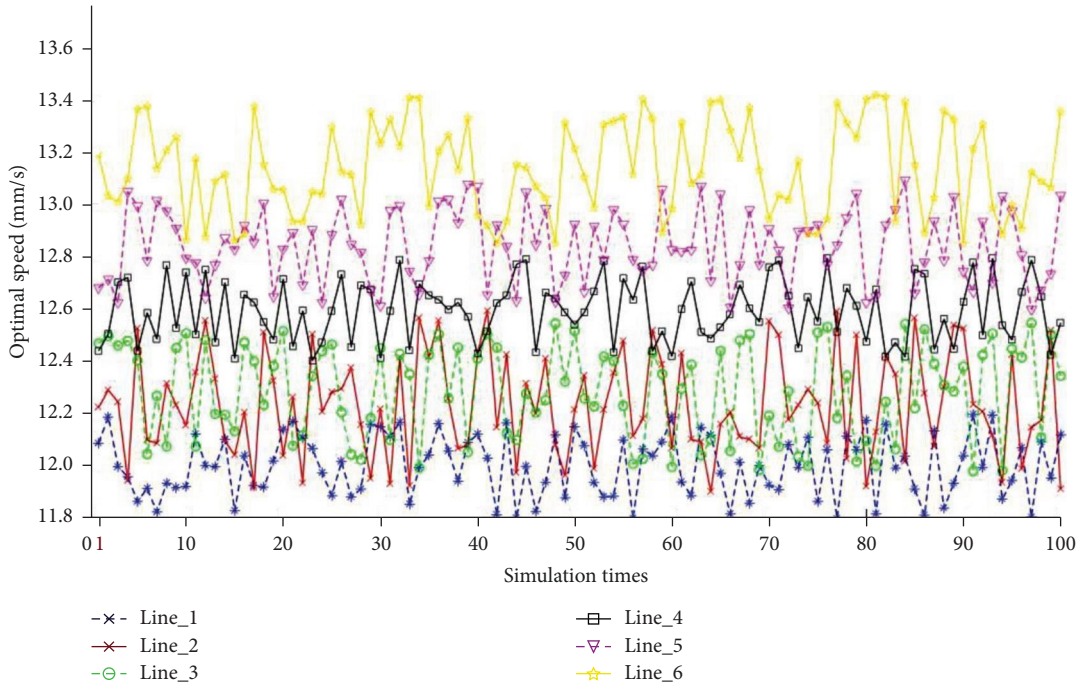

Figure 10: Simulation results of optimal puncture speed of prostate soft tissue (cancer) with different elastic modulus.

as possible), and a lot of this bionic soft tissue will be used in multiple puncture experiments. Therefore, the elastic moduli of the bionic soft tissues with each other will inevitably have slight differences in mass fabrication. Additionally, there is also a slight difference in the elastic modulus values between the fabricated bionic soft tissue and actual human prostate soft tissue. These slight differences may influence the discrepancy between the theory and experiment. However, the experimental results do not affect the theoretical analysis results; this result can be used as a verification of the theoretical model derivation, which proves that the trend of the theoretical model is consistent with that of the experimental data. To obtain more accurate experimental data and perform data optimization, this study adopts the method of taking the average value of multiple experiments to reduce the discrepancy between the theory and experiment, thus, the obtained experimental results are more in line with the theoretical derivation and practical requirements.

The result (12.60 mm/s) of the optimal puncture speed was obtained by experiments under the condition of the prepared silicone bionic soft tissue, thus, there was a certain deviation between the result and actual values. The data analysis combined the relevant simulation model established by the Urology Laboratory of Harbin Medical University using MATLAB and the puncture model in this study. It could be observed that these data depended on the age of the patient, and the parameters of the relevant model were different at different ages of the patients. After multiple simulation tests, the maximum range of the optimal puncture speed was $\sim 12.60 \pm 0.82$ mm/s, as shown in Figure 10. According to six groups of patients of different age groups with prostate cancer in the early and middle stages, the mean value of the elastic modulus of the prostate soft tissue was used for comparative testing, and the model of each group of elastic modulus values was simulated and iteratively optimized using an improved adaptive particle swarm algorithm (100 times for each group, 600 times in total). It can be observed from the figure that the average elastic modulus (79.82 MPa) of the prostate cancer cases (25 cases) of Chinese adult males aged from 55 to 64 years were used as the parameters to conduct 100 simulation tests, and the optimal puncture speed was obtained; the speed was between 12.60 ± 0.15 mm/s, and the punctured error was far less than 1.5 mm. Therefore, the puncture speed of 12.60 mm/s was chosen to meet the requirements of the best puncture speed, as shown in Line_4 in Figure 10.

Line_1 represents the data fluctuation line (optimal puncture speed) of the simulation optimization test of the model constructed for the average elastic modulus value (89.88 MPa) of the soft tissue of seven patients with prostate cancer aged from 25 to 34 years; Line_2 represents the data fluctuation line (optimal puncture speed) of the simulation optimization test of the model constructed for the average elastic modulus value (83.09 MPa) of the soft tissue for 12 patients with prostate cancer aged from 35 to 45 years; Line_3 represents the data fluctuation line (optimal puncture speed) of the simulation optimization test of the model constructed for the average elastic modulus value (81.57 MPa) of the soft tissue of 10 patients with prostate cancer aged from 46 to 54 years; Line_4 represents the data fluctuation line (optimal puncture speed) of the simulation optimization test of the model constructed for the average elastic modulus value (79.82 MPa) of the soft tissue of 27 patients with prostate cancer aged from 55 to 75 years; Line_5 represents the data fluctuation line (optimal puncture speed) of the simulation optimization test of the model constructed for the

average elastic modulus value (74.45 MPa) of the soft tissue of nine patients with prostate cancer aged from 76 to 84 years; Line_6 represents the data fluctuation line (optimal puncture speed) of the simulation optimization test of the model constructed for the average elastic modulus value (71.83 MPa) of the soft tissue of five patients with prostate cancer aged over 85 years.

The results, discussed in previous sections, further illustrate the following: in the process of puncturing prostate soft tissue, a faster puncturing speed is not the main requirement (compared with the conclusion from refs. [24, 27] that the faster, the better); an appropriate relative speed needs to be selected. Prostate cancer patients of different ages have different elastic moduli of the lesion site, and according to refs. [35, 36], it can be deduced that the incidence of prostate cancer is the highest for patients between the ages of 55 and 75 years. Therefore, choosing a puncture speed of 12.60 mm/s is also universal.

In the puncture experiment, although the optimized puncture speed can effectively improve the puncture performance, the puncture deviation still exists because of the fixed parameters of the puncture needle. Therefore, in future research work, it will be necessary to conduct in-depth research on the material properties, structural shape, and size parameters of medical puncture needles.

6. Conclusion

This study demonstrated that an appropriate puncture speed (12.6 mm/s) should be selected to ensure a good puncture effect during the puncturing of prostate soft tissue. The experimental results showed that this speed could reduce the puncture deviation caused by soft tissue deformation. In the case of different puncturing depths and continuous puncturing, a small puncturing positioning error and relatively stable puncturing accuracy can be maintained by this speed. The study provides design reference for the study of the positioning accuracy of minimally invasive puncture surgery.

Data Availability

The data used to support the findings of this study are included within the paper.

Conflicts of Interest

The authors declare that they have no conflicts of interest.

Funding

This research is partly supported by the National Natural Science Foundation of China (NSFC), project no. 51675142. Part of the fund was allocated by the key project ZD2018013 at the Natural Science Foundation of Heilongjiang, China. Part of the fund was allocated by GF Characteristic Discipline Construction Project of Harbin Institute of Technology: "Study on the integration mechanism modeling and high-fidelity multi-physical field coupling simulation of high energy efficiency EHA Electro-Hydrostatic actuator drive sensing control."

Acknowledgments

This work is supported and sponsored by Harbin Institute of Technology and Harbin Medical University.

References

[1] WHO, "Global health estimates 2020: deaths by cause, age, sex, by country and by region, 2000–2019," https://www.who.int/data/gho/data/themes/mortality-and-global-health-estimates/ghe-leading-causes-of-death.

[2] IARC, "Cancer Surveillance Branch (CSU)," https://www.iarc.who.int/branches-csu/.

[3] H. Sung, J. Ferlay, R. L. Siegel et al., "Global cancer statistics 2020: GLOBOCAN estimates of incidence and mortality worldwide for 36 cancers in 185 countries," *CA: A Cancer Journal for Clinicians*, vol. 71, no. 3, pp. 209–249, 2021.

[4] F. Bray, M. Colombet, L. Mery et al., *Cancer Incidence in Five Continents Volume XI*, IARC Scientific Publication, 2021, https://ci5.iarc.fr/ci5-xi/Default.aspx.

[5] Z. Liu, Z. Li, Y. Zhang et al., "Interpretation on the report of Global Cancer Statistics 2020," *Journal of Multidisciplinary Cancer Management (Electronic Version)*, vol. 7, no. 2, pp. 1–13, 2021.

[6] V. Agrawal, X. Ma, J. Kang, J. C. Hu, C. E. Barbieri, and H. Nagar, "Trends and disparities in the diagnosis and initial management of high-risk prostate cancer in the United States," *International Journal of Radiation Oncology, Biology, Physics*, vol. 108, no. 3, pp. e867–e868, 2020.

[7] R. L. Siegel, K. D. Miller, and A. Jemal, "Cancer statistics, 2020," *CA: A Cancer Journal for Clinicians*, vol. 70, no. 1, pp. 7–30, 2020.

[8] Y. Zhu, S. J. Freedland, and D. Ye, "Prostate cancer and prostatic diseases best of Asia, 2019: challenges and opportunities," *Prostate Cancer Prostatic Diseases*, vol. 23, pp. 197–198, 2020.

[9] Y. Zhang, B. Li, and L. Yuan, "Study on the control method and optimization experiment of prostate soft tissue puncture," *IEEE Access*, vol. 8, pp. 218621–218643, 2020.

[10] S. Elayaperumal, M. R. Cutkosky, P. Renaud, and B. L. Daniel, "A passive parallel master–slave mechanism for magnetic resonance imaging-guided interventions," *Journal of Medical Devices*, vol. 9, no. 1, Article ID 011008, 11 pages, 2015.

[11] B. Li, Y. Zhang, L. Yuan, and X. Xi, "Study on the low velocity stability of a prostate seed implantation robot's rotatory joint," *Electronics*, vol. 9, no. 2, Article ID 284, 2020.

[12] Y. Fu and B. Pan, "Research progress of surgical robot for minimally invasive surgery," *Journal of Harbin Institute of Technology*, vol. 51, Article ID 1, 2019.

[13] Y. Zhang, J. Peng, G. Liu, J. Jiang, and Y. Zhao, "Research on the segmentation method of prostate magnetic resonance image based on level set," *Chinese Journal of Scientific Instrument*, vol. 38, no. 2, pp. 416–424, 2017.

[14] D. S. Minhas, J. A. Engh, M. M. Fenske, and C. N. Riviere, "Modeling of needle steering via duty-cycled spinning," in *2007 29th Annual International Conference of the IEEE Engineering in Medicine and Biology Society*, pp. 2756–2759, IEEE, Lyon, France, 2007.

[15] A. Majewicz, J. J. Siegel, A. A. Stanley, and A. M. Okamura, "Design and evaluation of duty-cycling steering algorithms for robotically-driven steerable needles," in *2014 IEEE*

International Conference on Robotics and Automation (ICRA), pp. 5883–5888, IEEE, Hong Kong, China, 2014.

[16] Y. Sun, *Study on Robot-Assisted System for Percutaneous Surgery Based on 3D Ultrasound Images*, Harbin Institute of Technology, Harbin, 2011.

[17] Y. Sun, D. Wu, Z. Du, and L. Sun, "Robot-assisted needle insertion strategies based on liver force model," *Robot*, vol. 33, no. 1, pp. 66–70, 2011.

[18] Y. Liang, D. Xu, B. Wang, Y. Zhang, and Y. Xu, "Experimental study of needle insertion strategies of seed implantation articulated robot," *Journal of Mechanics in Medicine and Biology*, vol. 18, no. 3, Article ID 1850023, 2018.

[19] R. J. Webster, J. Memisevic, and A. M. Okamura, "Design considerations for robotic needle steering," in *Proceedings of the 2005 IEEE International Conference on Robotics and Automation*, pp. 3588–3594, IEEE, Barcelona, Spain, 2005.

[20] S. V. Pramod, F. Safriadi, Y. Kuddah, and R. R. Handoko, "Affordable novel device (VY) for transperineal prostate biopsy: a trial on prostate mannequin," *MethodsX*, vol. 8, Article ID 101417, 2021.

[21] Y. Jiang, *Finite Element Simulation and Experiment of Muscle Soft Tissue in Puncture Process*, Shandong University, Jinan, 2020.

[22] J. Fu, *Simulation of Coupling Process of Flexible Needle Insertion into Soft Tissue Based on ABAQUS*, Qinghai University, Xining, 2017.

[23] M. Li, *Research on Needle-Soft Tissue Interaction, Path Planning and Sensor Integration of Robotically Assisted Needle Placement*, Beijing Institute of Technology, Beijing, 2017.

[24] Y. Liang, *Research on Key Technology of Radioactive Seed Implantation Robot for Prostate*, Harbin University of Science and Technology, Harbin, 2017.

[25] P. Li, *Research on Key Technologies of MR Image-Guided Robot-Assisted Percutaneous Surgery*, Tianjin University, Tianjin, 2018.

[26] X. Zeng, *Finite Element Methods Simulation and Analysis of Needle Insertion Based on Virtual Crack Propagation*, Zhejiang University, Hangzhou, 2013.

[27] Y. Zhang, W. Zhang, Y. Liang, and Y. Xu, "Research on mechanism and strategy of high accuracy puncture of prostate," *Chinese Journal of Scientific Instrument*, vol. 38, no. 6, pp. 1405–1412, 2017.

[28] C. Cai, *Study on the Modeling and Analysis of Needle Bending and Tissue Deformation during Puncture and the Study of Puncture Puncture Path Planning*, Shandong University, Jinan, 2019.

[29] M. Mahvash and P. E. Dupont, "Mechanics of dynamic needle insertion into a biological material," *IEEE Transactions on Biomedical Engineering*, vol. 57, no. 4, pp. 934–943, 2010.

[30] M. Mahvash and P. E. Dupont, "Fast needle insertion to minimize tissue deformation and damage," in *2009 IEEE International Conference on Robotics and Automation*, pp. 3097–3102, IEEE, Kobe, Japan, 2009.

[31] S. Jiang, Z. Su, X. Wang, S. Liu, and Y. Yu, "Development of a new tissue-equivalent material applied to optimizing surgical accuracy," *Materials Science and Engineering: C*, vol. 33, no. 7, pp. 3768–3774, 2013.

[32] B. Li, *The Control Strategy and Experimental Study of the Motion Stationarity of the Agricultural Foot Mobile Platform*, Northeast Agricultural University, Harbin, 2018.

[33] H. Du, Y. Zhang, Y. Zhao, J. Jiang, and X. Jia, "Modeling of bevel-tipped needle inserting into soft tissue and estimation of needle tip trajectory," *Chinese Journal of Scientific Instrument*, vol. 36, no. 8, pp. 1744–1751, 2015.

[34] Y. Zhang, K. Shi, Y. Zhao, J. Yang, J. Liu, and L. Huang, "Study on force modeling and measurement for bevel tip flexible needle insertion into soft tissue," *Chinese Journal of Scientific Instrumen*, vol. 39, no. 6, pp. 164–172, 2018.

[35] D. Liang, *Human-Machine Interactive Control of Seed Implantation Robot for Prostate Based on Mixed Reality*, Harbin University of Science and Technology, Harbin, 2020.

[36] C. Xia, X. Dong, H. Li et al., "Cancer statistics in China and United States, 2022: profiles, trends,and determinants," *Chinese Medical Journal*, vol. 135, no. 5, pp. 584–590, 2022.